Laminar premixed flat non-stretched lean flames of hydrogen in air

Alekseev, Vladimir; Christensen, Moah; Berrocal, Edouard; Heimdal Nilsson, Elna; Konnov, Alexander

Published in:
Combustion and Flame

DOI:
10.1016/j.combustflame.2015.07.045

2015

Document Version:
Publisher's PDF, also known as Version of record

Combustion and Flame 162 (2015) 4063–4074

Contents lists available at ScienceDirect

Combustion and Flame

journal homepage: www.elsevier.com/locate/combustflame

Laminar premixed flat non-stretched lean flames of hydrogen in air

Vladimir A. Alekseev*, Moah Christensen, Edouard Berrocal, Elna J.K. Nilsson, Alexander A. Konnov

Division of Combustion Physics, Lund University, P.O. Box 118, SE-221 00, Lund, Sweden

ARTICLE INFO

Article history:
Received 13 May 2015
Revised 29 July 2015
Accepted 30 July 2015
Available online 19 August 2015

Keywords:
Hydrogen
Burning velocity
Heat flux method
Temperature dependence
Instability

ABSTRACT

Laminar burning velocity of lean hydrogen + air flames at standard conditions is still a debated topic in combustion. The existing burning velocity measurements possess a large spread due to the use of different measurement techniques and data processing approaches. The biggest uncertainty factor in these measurements comes from the necessity to perform extrapolation to the flat flame conditions, since all of the previously obtained data were recorded in stretched flames. In the present study, laminar burning velocity of lean hydrogen + air flames and its temperature dependence were for the first time studied in stretch-free flat flames on a heat flux burner. The equivalence ratio was varied from 0.375 to 0.5 and the range of the unburned gas temperatures was 278–358 K. The flat flames tended to form cells at adiabatic conditions, therefore special attention was paid to the issue of their appearance. The shape of the flames was monitored by taking OH* images with an EM-CCD camera. In most cases, the burning velocity had to be extrapolated from flat sub-adiabatic conditions, and the impact of this procedure was quantified by performing measurements in H_2 + air mixtures diluted by N_2. The effect of extrapolation was estimated to be of negligible importance for the flames at standard conditions. The measured burning velocities at 298 K showed an important difference to the previously obtained literature values. The temperature dependence of the burning velocity was extracted from the measured results. It was found to be in agreement with the trends predicted by the detailed kinetic modeling, as opposed to a vast majority of the available literature data.

1. Introduction

Since the early studies comparing measurements of the flame propagation in hydrogen + air mixtures and model predictions, e.g., [1,2], it was observed that even when a model agrees well with experimental results over a wide range of equivalence ratios, important disagreement remains for very lean near-limiting flames. Significant spread in the experimentally determined burning velocities obtained before 1980's was attributed to the impact of stretch and curvature, because all popular methods for measuring burning velocities, such as Bunsen burner or spherical flames, explored non-planar flame configurations. Nowadays, the importance of stretch correction in the interpretation of experimental data obtained in spherical or counterflow flames is well recognized, yet alarming disagreement is still not resolved [3,4]. This remaining disagreement in experimental determinations means that evaluation of the kinetic models at these conditions is highly uncertain.

Remaining scattering of the stretch-corrected burning velocities, S_L, obtained in lean hydrogen + air flames is illustrated in Fig. 1, which shows available data [5–23] at standard conditions, i.e., pressure of 1 atm and unburned gas temperature $T_g = 298$ K, and modeling results obtained with two recent hydrogen models [24,25]. The color codes denote the measurement method and stretch-correction model implemented: green – spherical flame, linear model [26]; blue – spherical flame, non-linear model of Kelley and Law [27]; red – counterflow burner, linear model (LM) originated from [28]; orange – counterflow burner, non-linear extrapolation (NLM) based on the study of Tien and Matalon [29] for the data of Das and Sung [22], and on the work of Wang et al. [30] for the data of Park et al. [23].

It is well known that lean hydrogen flames, even subject to stretch, are highly unstable. Bradley et al. [11] go as far as questioning the utility of S_L for these unstable flames, especially at high pressures. Formation of flame balls, an extreme limit of evolution of cellular instability, was suggested [31] to explain flame propagation beyond the theoretical 1D flammability limit, that was substantiated in microgravity experiments [32]. In contemporary experiments designed for measuring burning velocity in closed vessels (bombs), the onset of cellularity can be identified using shadowgraphy [11], Schlieren or tomography [18] techniques, and the propagating cellular flames are not considered in the data processing. The occurrence of cellularity limits the range of available raw data from these experiments to flames with relatively low radii and high stretch. This and other

* Corresponding author. Fax: +46462224542.
E-mail address: vladimir.alekseev@forbrf.lth.se, hedgefog@gmail.com (V.A. Alekseev).

http://dx.doi.org/10.1016/j.combustflame.2015.07.045
0010-2180/

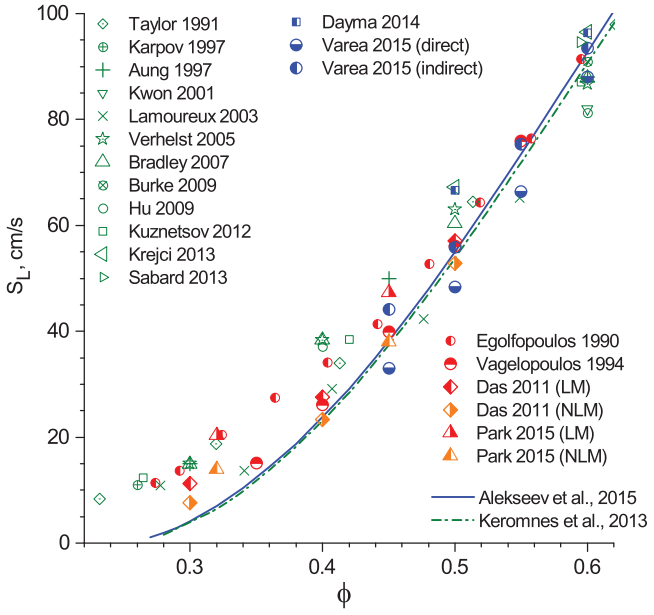

Fig. 1. Laminar burning velocity of H_2 + air flames at standard conditions ($T_g = 298$ K, $p = 1$ atm). Symbols: experiments, lines: calculations using models from [24,25]. The source of experimental data: green - Taylor [5], Karpov et al. [6], Aung et al. [7], Kwon and Faeth [8], Lamoureux et al. [9], Verhelst et al. [10], Bradley et al. [11], Burke et al. [12], Hu et al. [13], Kuznetsov et al. [14], Krejci et al. [15], Sabard et al. [16]; blue - Dayma et al. [17], Varea et al. [18]; red - Egolfopoulos and Law [19], Vagelopoulos et al. [20], Das et al. [21], Park et al. [23]; orange – Das et al. [22], Park et al. [23]. (For interpretation of the references to color in this figure legend, the reader is referred to the web version of this article.)

experimental challenges discussed by Egolfopoulos et al. [33] could, at least partly, be responsible for the large data scattering depicted in Fig. 1.

Proper stretch-correction is probably the most important issue affecting the burning velocity derived from counterflow or spherical flames. Direct comparison of the measurements performed in counterflow configuration by Das et al. and processed using linear [21] or non-linear model [22] shows that non-linear extrapolation yields S_L about 32% lower when equivalence ratio, ϕ, equals 0.3. At $\phi = 0.4$, however, these models produced results closer to each other and to the measurements of Vagelopoulos et al. [20], see Fig. 1. In the most recent study of H_2 + air flames using counterflow technique, Park et al. [23] demonstrated that non-linear extrapolation lowers the S_L values significantly in lean flames with $\phi = 0.32$ and 0.45 as compared to the linear model.

The situation in analysis of spherical flame experiments is even more upsetting. As was shown in the recent study of Wu et al. [34], all existing methods for stretch correction in the spherical flame configuration, which was employed to get the vast majority of data in H_2 + air flames, overestimate the laminar burning velocity, and for the classical linear model [26] the difference can reach up to 60%. Other effects related to highly diffusive nature of H_2 and applicability of the calculated density ratio between cold reactants and products to convert flame displacement speed into burning velocity were addressed by Varea et al. [18]. The authors used the technique for direct measurement of the local instantaneous unburned gas velocity [35,36] (denoted "direct" in Fig. 1) and compared the results obtained to S_L determined with a common approach by assuming jump conditions across the flame (denoted "indirect" in Fig. 1). It was clearly demonstrated that these two methods lead to different values of S_L, with the discrepancy increasing when equivalence ratio decreases, even though the numerical simulations predict similar values for the two formulations.

To avoid the impact of stretch correction, independent measurements of the laminar burning velocity of H_2 + air mixtures using flat non-stretched flames could be most useful. This was the first goal of the present study, since no measurements with hydrogen burning in air and stabilized on the heat flux burner were performed so far. There are, however, several investigations of S_L in diluted H_2 flames. The first experiments in $H_2 + O_2 + N_2$ mixtures were done by Hermanns et al. [37]. The authors compared the data obtained in flat flames to the earlier counterflow measurements of Egolfopoulos and Law [19]. The amount of O_2 in the oxidizer, $O_2 + N_2$, was from 7 to 11%, and the equivalence ratio was varied in the range $\phi = 0.65$–3.1. Ratna Kishore et al. [38] also used the heat flux method and studied the effect of dilution by Ar, N_2 and CO_2 on $H_2 + O_2$ flame propagation. They found that lean and stoichiometric CO_2-diluted flames (65% in the total mixture) become cellular, whereas Ar and N_2-diluted flames remained flat. For N_2, the dilution ratios were similar to [37] and direct comparison to 7.7% O_2 flames of [37] showed good agreement in S_L. Voss et al. [39] studied diluted H_2 flames, adding N_2 to the fuel and mixing it with air. If expressed the same way as by Hermanns et al. [37], the studied range covered O_2 content from 6 to 17.7%, and ϕ was varied from 0.45 to 1.5. In the absence of stretch, hydrogen flames stabilized on the heat flux burner are prone to cell formation, especially at higher pressures. Goswami et al. [40] measured burning velocities of syngas and hydrogen up to 10 atm, and had to use O_2 + He oxidizer mixture to suppress cellularity in lean flames. Yu [41] showed numerically that for a typical burner geometry and operating conditions, lean ($\phi = 0.56$) $H_2 + O_2 + N_2$ flame with 18% O_2 in the oxidizer is subject to thermal-diffusive instability. Yu et al. [42] further concluded that in order to increase the stability and obtain an adiabatic flame on a heat flux burner, the flame has to be brought closer to the burner surface below what was called "a critical stand-off distance". For a mixture of given composition, this can be achieved by decreasing the unburned gas velocity and moving to sub-adiabatic conditions. In the present work, special attention was paid to the cell appearance in the premixed hydrogen flames due to its possible effect on S_L.

In addition to the spread in S_L, observed in Fig. 1, another serious issue related to lean H_2 + air flames was identified in our recent study [25]. It concerns the temperature dependence of the laminar burning velocity, commonly evaluated in the form of an empirical power law:

$$S_L = S_L^0 (T_g/T_0)^{\alpha}, \quad (1)$$

where S_L^0 is the burning velocity at a reference temperature T_0, and α is the power exponent. It was found that for very lean H_2 + air mixtures ($\phi < 0.5$), all available data obtained in spherical vessels fail to confirm the rise of the temperature exponent α anticipated close to the flammability limit and predicted by kinetic modeling. Only power exponent α extracted from the measurements of Das et al. [21,22], a single counterflow study performed at elevated temperature, followed the modelling trend, however, with rather high uncertainty, since this study [21] was not aimed at revealing the temperature dependence due to very narrow temperature range (25 K). Thus the second goal of the present work was to study the temperature dependence of S_L in lean H_2 + air flames with the aim to resolve the discrepancy observed in [25], and in addition, to identify whether the temperature exponent α can serve as a criterion of reliability and consistency of the burning velocity measurements.

2. Experimental details

The laminar burning velocity of lean H_2 + air mixtures and its temperature dependence was determined with the heat flux method covering the equivalence ratios of $\phi = 0.375$–0.5 and unburned gas temperatures $T_g = 278$–358 K. The latter range is conditioned by the use of water as a temperature controlling agent. The range of

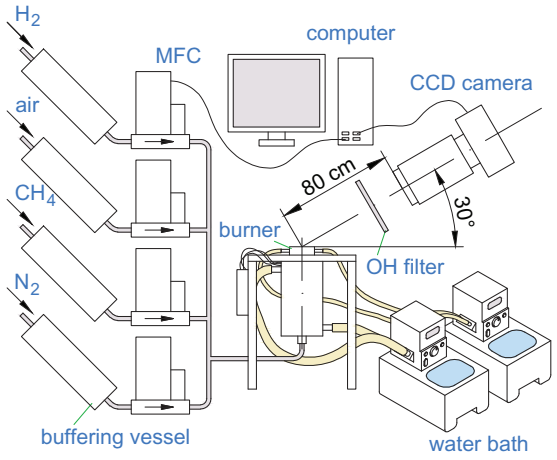

Fig. 2. Schematic of the experimental setup, not to scale.

unburned gas velocities, where the flame geometry remains one-dimensional, for the burner configuration employed in the present study was evaluated to be 10 cm/s $\leq V_g \leq$ 50 cm/s [43], or below 40 cm/s [44]. Hermanns [45] specified this range to be $\leq$ 60 cm/s in relation to the measurements in [37]. These recommendations are associated with the tolerated increase of the flame surface, typically by 0.5%, as discussed by Goswami et al. [46]. In the present work, gas velocities from 9 cm/s up to 55 cm/s were considered in the determination of S_L of H_2 + air mixtures, corresponding to the boundary values of equivalence ratio of 0.4 and 0.5, respectively. H_2 + air mixtures diluted by N_2 with $O_2/(O_2 + N_2) = 0.1077$ were also studied in the range of equivalence ratios of $\phi = 0.77$–0.97 and unburned gas temperatures $T_g = 298$–358 K.

The measurements were performed on the experimental setup shown in Fig. 2. The essential parts of the current installation are similar to those described by Bosschaart and de Goey [43], while with notable differences in the data processing procedure, as will be elucidated in the following. The gases, H_2 and air (AGA Gas AB, air composition 21% O_2, 79% N_2, H_2 purity 99.9%), are fed from the central supply system, and flow rates are set by Bronkhorst mass flow controllers (MFC), operated from a computer through a LabView interface. Diluted mixtures were obtained by mixing air with respective amount of N_2 (AGA Gas AB, purity 99.996%). Buffering vessels are installed upstream of the MFCs, damping possible fluctuations in the inlet flows. For the convenience of ignition and flame control, methane (CH_4) is added to the mixture at the first stage and is gradually removed before the start of the actual measurements. For the reliable transfer between the equivalence ratios in the flames that can not be directly observed, it is performed by a slow step-wise change of the flow rates controlled by the LabView script.

The gases are fed into the plenum chamber of the burner through a long teflon tube allowing time for complete mixing. The required unburned gas temperature is set by a thermostatic water bath which creates a circuit around the plenum chamber. For the low temperature measurements at 278 K, the water in the bath was externally cooled using ice and liquid nitrogen. A second water bath keeps the temperature of the burner plate at 368 K, through a heating jacket on the burner head, as shown in a schematic of the burner in Fig. 3.

In a single measurement of the burning velocity, the unburned gas speed is varied in a certain interval, and when it is increased, starting from some value the flames become corrugated. Since H_2 flames do not emit in the visible region, this process cannot be directly observed. Therefore, the shape of the flames was monitored by imaging the OH^* emission using an EM-CCD camera (Andor Luca DL-604M-OEM) sensitive at $\lambda = 310$ nm and a bandpass filter. The transmittance window of the filter was ca. 250–400 nm, therefore all H_2O radiation in the product zone was effectively blocked, making it possible to resolve the flame front. The images were recorded from an angle of 30° (see Fig. 2), so that the instability region could be located on the burner plate. Due to relatively low signal, the resulting images were accumulated over about 10–20 s. Such procedure was possible since the cells forming in the flame structure were stable in time.

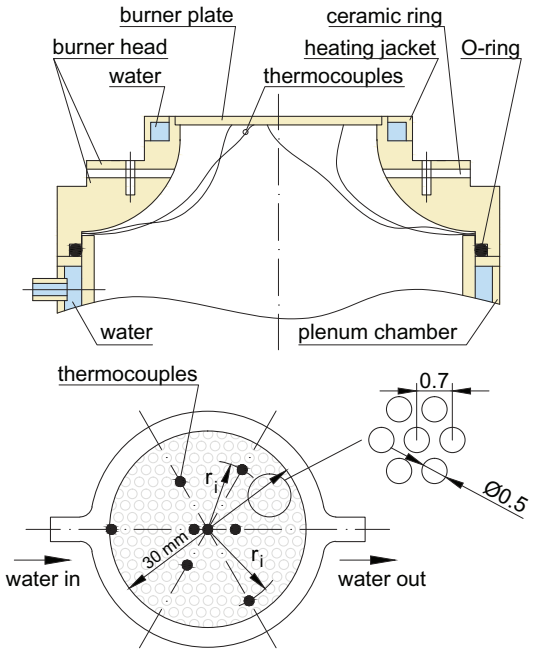

Fig. 3. Cross-section and top view of the heat flux burner head.

The configuration of the burner used for the present measurements is shown in Fig. 3. It largely repeats the design introduced in [43]. A 2 mm perforated burner plate is attached with thermal glue to the burner head, which is kept preheated by a water jacket. The top part of the burner head is insulated from the bottom part and the plenum chamber with a ceramic ring. The temperature distribution in the burner plate is monitored by a set of 0.13 mm unshielded T-type thermocouples (TC), directly attached to the holes of the burner plate.

In the heat flux method, the adiabatic conditions are achieved when heat loss to the burner from the flame, necessary for its stabilization, is compensated by a heat gain to the unburned mixture when it enters the preheated burner plate. Van Maaren et al. [47] developed analytical expression for the temperature distribution in the burner plate, which was later presented [48] in a simplified form:

$$\bar{T}_p(r) = T_{center} - \frac{q}{4\lambda h} r^2, \tag{2}$$

where T_{center} is the temperature of the central point, q is the net heat transfer per unit area to (from) the burner plate, λ is the thermal conductivity of the burner plate in radial direction and h is the width of the plate. The net heat transfer q is a difference between the heat gain to the burner plate from the flame (q_+) and the heat loss to the preheating gas (q_-), i.e.:

$$q = q_+ - q_-. \tag{3}$$

The quantity $-q/(4\lambda h)$ is called the parabolic coefficient, C, and it is the key parameter of the method. It is obtained from the measured temperature distribution in the burner plate. Consequently, when the flow rate of the cold mixture is adjusted, it affects q, and adiabatic conditions, i.e. $q = 0$, can be identified by observing constant temperature profile in the burner plate (see Eq. (2)). The laminar burning velocity, S_L, is then calculated from the total flow rate set by the MFCs. The flow surface area A, required to convert the total flow rate into gas

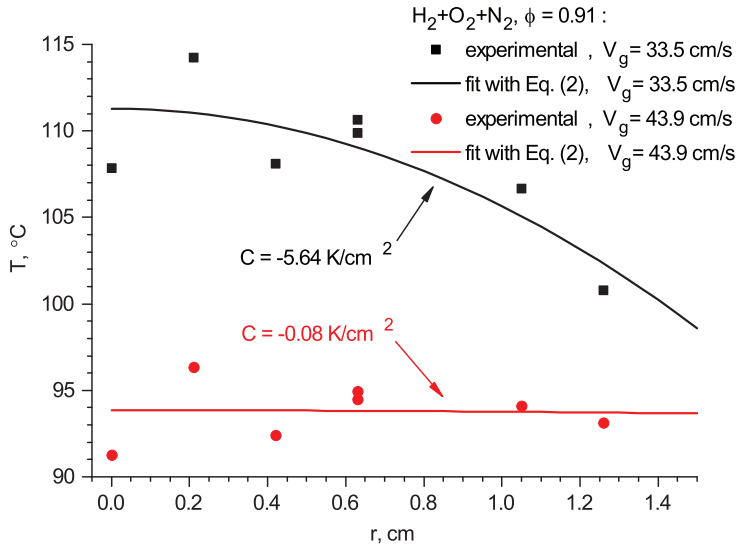

Fig. 4. Temperature distribution in the burner plate for $H_2 + O_2 + N_2$ flame ($O_2/(O_2 + N_2) = 0.1077$) at $\phi = 0.91$, $T_g = 318$ K and $V_g = 33.5$ cm/s (black), $V_g = 43.9$ cm/s (red). Symbols: experimental, line: parabolic fit with Eq. (2). (For interpretation of the references to color in this figure legend, the reader is referred to the web version of this article.)

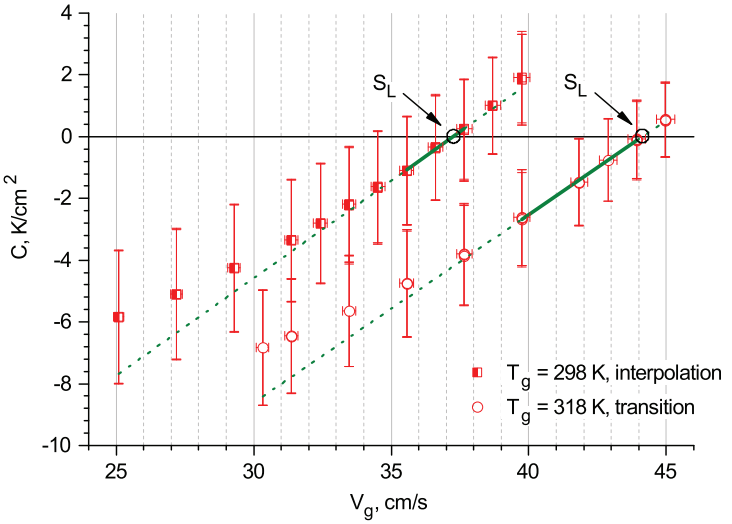

Fig. 5. Determination of S_L from the $C(V_g)$ dependence for two $H_2 + O_2 + N_2$ flames with $O_2/(O_2 + N_2) = 0.1077$ at $\phi = 0.91$ and $T_g = 298$ and 318 K.

velocity, was defined as the area covered by the perforation pattern, and this area was found to be 5.25% smaller than the upstream burner cross section area (ID = 3 cm). In the data processing, the surface area of the perforation was used.

3. Data processing and error analysis

3.1. Determination of S_L

A typical procedure for measurements of the burning velocity in flat flames stabilized at adiabatic conditions consists of determining the parabolic coefficient C as a function of cold gas velocity V_g. To illustrate this procedure, Fig. 4 shows two temperature profiles for a diluted mixture with $O_2/(O_2 + N_2) = 0.1077$ at $\phi = 0.91$ and $T_g = 318$ K. All mixtures with 10.77% O_2 in the oxidizer are denoted "H_2+O_2+N_2" in Fig. 4 and following Figures. The profiles correspond to sub-adiabatic conditions ($V_g = 33.5$ cm/s, $C = -5.64$ K/cm^2) and conditions near adiabatic ($V_g = 43.9$ cm/s, $C = -0.08$ K/cm^2). The lines in Fig. 4 represent the fits of the experimental temperature profiles to Eq. (2) made with a linear regression in T-r^2 coordinates. Note that at the edge of the burner plate, i.e. at $r = 1.5$ cm, both lines are close to $T = 95$° C, which is the set temperature of the heating water jacket.

In a typical heat flux experiment, after recording the $C(V_g)$ dependence, the location of $C = 0$, $V_g = S_L$ is found by linear interpolation of the points in the vicinity of these conditions. Figure 5 illustrates the process for the same mixture as in Fig. 4 at two temperatures: $T_g =$ 298 K and $T_g = 318$ K. The points used for S_L determination are fitted linearly, as shown by the thick green lines. At $T_g = 298$ K, S_L is obtained by interpolation. At 318 K, the flames started to become corrugated around adiabatic conditions, therefore, the super-adiabatic point $V_g = 45$ cm/s was not included into the fitting domain, and S_L was obtained by extrapolation. However, the last sub-adiabatic point lies very close to $C = 0$ (see also Fig. 4), i.e., closer than the distance between two measured points. The general method of S_L determination is still valid, and in Fig. 5 it is referred to as "transitional" to extrapolation. Green dot lines show extrapolation of the fitted line to all recorded points with the aim to visualize the behavior of $C(V_g)$ in sub-adiabatic conditions.

A local linearity of $C(V_g)$ is always assumed, with the parabolic coefficient sensitivity s, which is the slope of the line, being one of the main parameters determining the accuracy of the measurements

[43]. While it is known that s varies with burner plate material [48], geometrical parameters (Eq. (2)), and with equivalence ratio [49], it was also found to be weakly dependent on the type of the fuel for the case of lower alkanes [49]. The exact functional dependence $C(V_g)$ for wider sub- and super-adiabatic domains will be presented below, however, the assumption of local linearity is sufficient for S_L determination provided that the flame is stable. However, as can be inferred from Fig. 5, as well as from the results presented by Bosschaart and de Goey [43] and by Knorsch et al. [50], $C(V_g)$ becomes non-linear at some point below the adiabatic conditions, with the decreasing sensitivity s. From Fig. 5 it is evident that if only the lowest sub-adiabatic velocities were available, S_L would be significantly overestimated.

Thus, the non-linearity of $C(V_g)$ becomes important when the laminar burning velocity of H_2 + air flames is measured, since for most of the measured cases (ϕ and T_g), the flames at adiabatic conditions were cellular, or were even never observed due to a break in $C(V_g)$ linear dependence and noticeable decrease in s. This change occurred at a point where cells became fully developed and then merged together to form a labyrinth-like structure (For examples, see images in Supplemental material). Therefore, the burning velocity had to be extrapolated from sub-adiabatic conditions where the flames were flat. A notable observed difference of H_2 flames from the hydrocarbon fuels was a decreased value of sensitivity s for the same range of gas velocities ($s = 0.4$–0.5 K/cm^2 for H_2 + air flames at 298 K, which can be compared to $s = 1$–2.5 K/cm^2 from, e.g., [49,51], obtained on burners with the same geometrical parameters).Therefore, the extrapolation had to be performed to a comparably larger interval of velocities, and non-linearity in $C(V_g)$ might have had a significant effect on extrapolated values of S_L.

Bosschaart and de Goey [52] developed an analytical expression for s based on Zeldovich theory of flame propagation [53], and it was found to be dependent on several flame and burner plate characteristics including adiabatic flame temperature T^{ad} and Zeldovich number Ze. In the following, $C(V_g)$ and s will be determined based on the approach of the pioneering work of Botha and Spalding [54], who proposed that the heat transfer to the burner is equivalent to pre-cooling of the initial mixture if no reactions occur upstream of the burner surface. From Eq. (2), the total amount of heat transferred to the burner, Q:

$$Q = -4\lambda h A \cdot C, \tag{4}$$

where A is the burner surface area. Q is equal to the heat released by cooling the initial mixture by temperature ΔT:

$$Q = -\frac{p_0}{RT_g} V_g A \cdot c_p^v \cdot \Delta T, \tag{5}$$

where c_p^v is the mixture molar heat capacity, p_0 is ambient pressure and R is the gas constant.

At the same time, the non-adiabatic flame with the heat loss Q to the burner, as proposed in [54], is equivalent to adiabatic flame at temperature $T_g' = T_g + \Delta T$, therefore, Eq. (1) can be used to write:

$$S_L' = S_L \left(\frac{T_g + \Delta T}{T_g} \right)^{\alpha}, \tag{6}$$

where S_L and S_L' are burning velocities at temperatures T_g and T_g', respectively. Finally, since the total mass flow is constant, then:

$$\frac{S_L'}{T_g + \Delta T} = \frac{V_g}{T_g}. \tag{7}$$

Combining Eqs. (5)–(7), the parabolic coefficient C becomes equal to:

$$C = \frac{p_0}{4\lambda h R} \cdot c_p^v \cdot V_g \cdot \left[\left(\frac{V_g}{S_L} \right)^{\frac{1}{\alpha - 1}} - 1 \right], \tag{8}$$

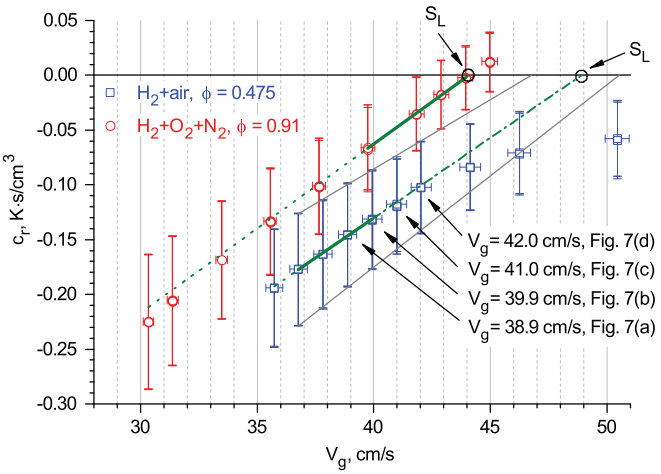

Fig. 6. Determination of S_L from the c_r dependence for H_2 + air flame at 318 K and $\phi = 0.475$ (blue) and $H_2 + O_2 + N_2$ flame with $O_2/(O_2 + N_2) = 0.1077$ at 318 K and $\phi = 0.91$ (red). (For interpretation of the references to color in this figure legend, the reader is referred to the web version of this article.)

and the sensitivity s at $V_g = S_L$:

$$s = \left. \frac{dC}{dV_g} \right|_{V_g = S_L} = \frac{p_0}{4\lambda h R} \cdot c_p^v \cdot \left(\frac{1}{\alpha - 1} \right). \tag{9}$$

The decreased sensitivity s in H_2 + air flames, according to Eq. (9), is due to increase of α. As will be shown in Section 4.4, for the studied H_2 + air flames, $\alpha = 3$–4, compared to a value around 1.5 in stoichiometric hydrocarbon flames. Eq. (9) also explains the decrease of s in lean or rich hydrocarbon flames observed in, e.g., [49].

As a result of the need for extrapolation, a modified method of the data processing was used in the present study. Instead of directly plotting C as a function of V_g, a normalized relative quantity $c_r = C/V_g$ was used. The approach is based on the work of Botha and Spalding [54], who used a porous plug burner and determined S_L by recording the amount of heat transferred from the flame to the cooling water. The data were then extrapolated to zero loss conditions. They plotted the heat loss normalized over a volume of fuel and found that the obtained curves were linear in very wide ranges of cold gas velocities. For the case of the present study, this quantity is equivalent to c_r since $C \sim q$ and V_g is proportional to volumetric fuel flow for a given ϕ and T_g. However, Botha and Spalding [54] did not have a possibility to check the linearity assumption, since an adiabatic flame would not stabilize on their burner. In the current work, the issue of c_r linearity, and consequently, the influence of extrapolation on the obtained S_L of H_2 + air flames were investigated by performing additional measurements in stable diluted flames and linking the two sets of mixtures with an approach described in detail below.

Examples of the procedure of S_L determination from the measured c_r data is illustrated in Fig. 6 for two cases: H_2 + air flame with $\phi = 0.475$ and $H_2 + O_2 + N_2$ flame with $O_2/(O_2 + N_2) = 0.1077$ and $\phi = 0.91$, both at $T_g = 318$ K. In the latter mixture, denoted by red circles, a point at conditions very close to adiabatic is available, which is not the case for H_2 + air flame (blue squares). No super-adiabatic points ($c_r > 0$) exist due to corrugation of the flame and subsequent decrease of the slope of the c_r dependence. Therefore, the points where the flames are not flat had to be filtered out, and based on the remaining points, S_L had to be obtained by fitting the extrapolation line. The filtering was done using the corresponding images of OH* emission recorded simultaneously to the parabolic coefficient measurement. Figure 7 gives an example of these images for the H_2 + air flame of Fig. 6. The position of the holes blocked by the thermocouples is seen on the images as "dips" in the flame front on the radii located at 60° to each other. Generally, the instabilities start to grow

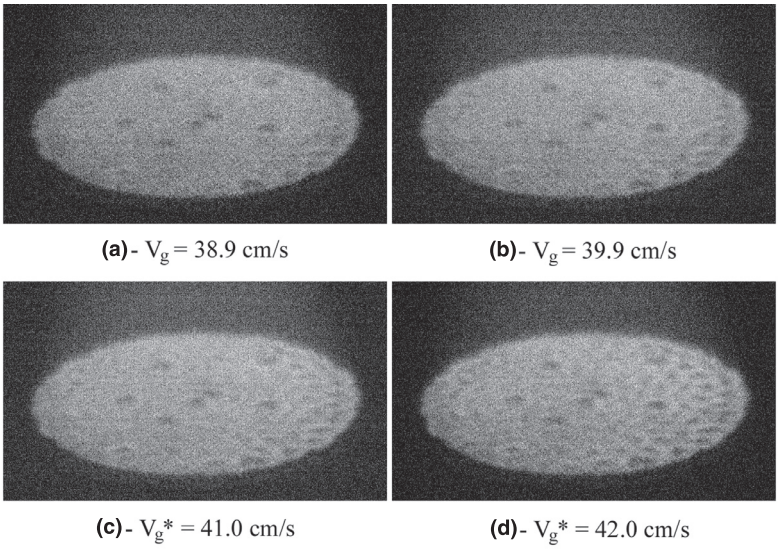

Fig. 7. Images of the OH* emission in the H_2 + air flames at $\phi = 0.475$ and $T_g = 318$ K for different cold gas velocities V_g. The asterisks denote velocities filtered out due to growing corrugation.

at the right side of the burner (Fig. 7c), possibly because the thermal contact between the burner plate and burner head can not be made ideally uniform for the present burner design. At that time, most of the flame is still undisturbed, while with further increase of V_g, the corrugation spreads over the whole flame front (Fig. 7d). In the data processing, points with small localized instabilities were considered in the measurements, since they did not affect the parabolic coefficient. For instance, in Figs. S9, S10 of the Supplemental Material it can be seen that c_r is linear from 31 to 42 cm/s for the flame at $\phi = 0.5$, $T_g = 278$ K, covering flat, locally corrugated and corrugated conditions. The conditions with developed corrugation were filtered out. For the case of H_2 + air flame in Figs. 6 and 7, the points corresponding to Fig. 7a,b ($V_g = 38.9$ and 39.9 cm/s) were kept and higher velocities were removed (Fig. 7c,d, $V_g = 41$ and 42 cm/s). Note that the last point for the diluted mixture ($V_g = 45$ cm/s) was also removed due to the grown instabilities. The noticeable change of the slope in H_2 + air flame occurs at ca. 45 cm/s where cells start to merge with each other.

In Fig. 6, similarly to Fig. 5, points used for S_L determination in H_2 + air mixture are fitted with thick green line, which is further extrapolated to $c_r = 0$ (dash-dot green line). For $H_2 + O_2 + N_2$ mixture, the extrapolation back to sub-adiabatic flames is denoted with green dot line to visualize the linearity of c_r dependence. Comparing Figs. 5 and 6, it can be seen that the relative parameter c_r shows a linear dependence much longer than the original $C(V_g)$. This also follows from the behavior of Eq. (8), since it can be easily shown that for any $a > 0$, a dependency of the form $x \bullet (x^a - 1)$ has a larger curvature than $(x^a - 1)$ at $x = 1$, where $x = V_g/S_L$ from Eq. (8).

The extrapolation was typically performed using 4 experimental points (if available), which was found to be sufficient to reduce random scatter occurred in the recorded c_r. On the other hand, in a wider range c_r start to deviate from a straight line due to a systematic nonlinear behavior (see the red symbols and dot line in Fig. 6), therefore, the lower velocities were also removed from the extrapolation domain. In the Supplemental material, the procedure of c_r filtering and S_L determination is presented for all considered flames, and the evolution of the cell structure is illustrated by OH* images.

For the H_2 + air flame in Fig. 6, the corrugation began ~3 cm/s before the noticeable change of the slope of $C(V_g)$. Generalizing over all H_2 + air mixtures, it occurred at velocities about 10–15% above the last value where corrugation was still localized, i.e. the last point used for S_L determination. These higher velocities of the linear part of the curve were removed at the data processing stage. Nevertheless, it does not affect significantly the slope of the extrapolation line, as evident from Fig. 6. If these points were considered in the data processing, the corresponding S_L values would increase generally by about 2–4%.

3.2. Error analysis

Two major sources of uncertainty are generally associated with the burning velocity measurement using the heat flux method: the accuracy of V_g, which is dependent on the uncertainty in the flow rates and the unburned gas temperature, and the accuracy of the determination of the parabolic coefficient C, characterized by the scattering in the recorded temperature profiles. In the current study, an additional source of error is present, arising from the extrapolation procedure. In the following, each of the three contributions will be discussed separately.

The total errors in cold gas velocity V_g and equivalence ratio originate from the accuracy of the flow rate measurement, and they constitute from errors in the flow rates of each mixture component. The MFCs were calibrated prior to measurements, with air and H_2, respectively, using MesaLabs DryCal Definer 220 positive displacement flow meter for air and Defender 530 for H_2. Calibration curves in the form of third or fourth degree polynomials were introduced into the LabView operating program and used for the correction of the flow rates before they are sent to MFCs. Therefore, the uncertainty in each flow rate is a sum of ±1% accuracy of Definer 220 or ±1.2% for Defender 530 plus the stated flow repeatability of the MFC, which equals to 0.2%. Combined in a square sum for H_2 and air flow rates, it results in a total error in ϕ of about 1.8%. For V_g, since air is a major component in the mixture, the total error was comparable to the error in the air flow (±1%). The accuracy of V_g is indicated by horizontal error bars in Figs. 5 and 6. After the measurements, the calibration of the air MFC was repeated with a Ritter TG10 drum-type gas meter in order to check for possible systematic drifts from the stated flow repeatability. The difference between calibration curves from Definer 220 and Ritter TG10 drum was found to be well within the stated uncertainty interval of ±1% for the Definer 220.

The uncertainty in S_L caused by the temperature of the unburned gas T_g was also evaluated. Since the gas velocity V_g is not measured directly but calculated from the mass flow, it is proportional to T_g, which is set by the controller of the water bath. The uncertainty in T_g affects S_L in the same way as the uncertainty in V_g caused by the MFCs. At the same time, $S_L \sim (T_g)^{\alpha}$ (see Eq. (1)), therefore, the burning velocity at the desired temperature T_0 is proportional to $T_g^{(1-\alpha)}$. Consequently, the uncertainty in the burning velocity is $\Delta S_L/S_L = (1-\alpha)\cdot\Delta T_g/T_g$. As will be shown in Section 4.4, in the lean H_2 + air flames considered, α is about 3–4. The sensor of the water bath has a scale of 0.1 K, yet, even if the uncertainty is about ±0.5 K, its influence on S_L does not exceed 0.5%. Therefore, it was not considered in the total error estimation.

Scattering in the recorded temperature profiles results in the uncertainty of the parabolic coefficient C, and subsequently in c_r, as indicated by vertical error bars in Figs. 5 and 6. Note that even though $c_r = C/V_g$ also includes the gas velocity, its uncertainty does not affect the intersection with the zero line $c_r = 0$, since for a constant relative uncertainty in V_g, as it is defined above, the uncertainty interval of c_r will be converging to a single point when c_r approaches zero. Also, the relative uncertainty in V_g is at least one order of magnitude smaller than in C. Therefore, it affects S_L only through the horizontal error bars as in Fig. 6.

The observed thermocouple (TC) scattering from the fit to Eq. (2) generally exceeded the instrumental accuracy, therefore the uncertainty in the parabolic coefficient, σ_C, could not be calculated with the original method of [43] and was estimated with an approach recently presented by the authors [51]. Since C is obtained from linear regression of the measured burner plate temperature as a function of the squared radius r^2 (Eq. (2)), the standard error of C was considered as its uncertainty, σ_C. This quantity is a characteristic of the burner, since it was found to be practically constant. It also corresponds to the values measured with this burner in hydrocarbon fuels (as was concluded based on series of measurements in CH_4, CH_3OH or C_2H_5OH as well as on previously reported data [51]). The difference therefore comes from the slope of c_r curve, the sensitivity of the parabolic coefficient, whose decrease was found to be the main reason for increased error bars compared to other fuels. The influence of the TC scattering on S_L is depicted in Fig. 6 by gray lines. Since the errors from TC scattering in each point are dependent, the errors were added/subtracted to/from c_r, and the resulting values were used for S_L extrapolation. This resulted in asymmetrical errors in S_L, larger on the negative side. Also, since σ_C was close to constant, the errors decreased with increasing S_L.

The influence of the third source of uncertainty, the extrapolation of S_L, was estimated as the following. According to Eq. (8), the $C(V_g)$ in stable flat flames on a particular burner depends on the burning velocity S_L, temperature exponent α and molar heat capacity c_p^{ν}. Therefore, if two arbitrary mixtures have all these parameters in common, then the shape of c_r as a function of V_g can also be expected to be similar. For the case of lean H_2 + air flames, such a counterpart was found in diluted flames. The five H_2 + air mixtures measured in the present work were associated with corresponding $H_2 + O_2 + N_2$ mixtures ($O_2/(O_2 + N_2) = 0.1077$), which had the same mole fraction of H_2, and their properties are listed in Table 1 for $T_g = 298$ K. The heat capacities of H_2, N_2 and O_2 are similar, therefore, there is no difference in c_p^{ν} for all mixtures. Burning velocities and temperature exponents are calculated with the detailed mechanism for H_2 combustion [25]. It can be seen that all quantities are very similar for the two sets of mixtures.

The resemblance of the counterpart mixtures in terms of shape and location of the c_r curves in V_g-c_r coordinates can be assessed from Fig. 6. It can be seen that the slope of the two c_r dependencies is identical and the velocity range is similar. The corresponding figures for other mixtures are presented in the Supplemental material. Here it has to be emphasized that the proposed method was not intended to "correct" the obtained S_L for extrapolation, the aim was to estimate the degree of introduced uncertainty.

Table 1
Comparison of the properties for the H_2 + air and $H_2 + O_2 + N_2$ ($O_2/(O_2 + N_2) = 0.1077$) mixtures at 298 K.

N	mixture	ϕ	%H_2	S_L, cm/s	α	c_p^{ν}, J/(mol•K)
1	H_2 + air	0.4	14.4	23.8	2.79	29.12
	$H_2 + O_2 + N_2$	0.77	14.2	21.9	2.85	29.10
2	H_2 + air	0.425	15.1	30.6	2.62	29.12
	$H_2 + O_2 + N_2$	0.82	15	28.4	2.71	29.09
3	H_2 + air	0.45	15.9	38.1	2.54	29.11
	$H_2 + O_2 + N_2$	0.86	15.6	34.0	2.59	29.09
4	H_2 + air	0.475	16.6	46.3	2.41	29.11
	$H_2 + O_2 + N_2$	0.91	16.4	41.5	2.45	29.09
5	H_2 + air	0.5	17.4	55.0	2.32	29.11
	$H_2 + O_2 + N_2$	0.97	17.3	50.8	2.30	29.09

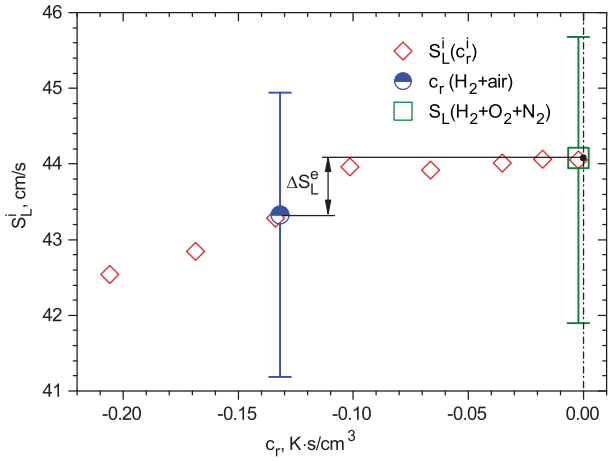

Fig. 8. Determination of the ΔS_L originating from extrapolation. The symbols are: $S_L{}^i(c_r{}^i)$ – red diamonds; real S_L of $H_2 + O_2 + N_2$ mixture – green square; the position of c_r of the H_2 + air mixture – blue circle. The error bars correspond to S_L uncertainty from TC scattering. The distance ΔS_L^e corresponds to the extrapolation uncertainty. (For interpretation of the references to color in this figure legend, the reader is referred to the web version of this article.)

The influence of extrapolation is illustrated in Fig. 8 for the two flames of Fig. 6. The experimental c_r dependence for the diluted mixtures was used, where the real value of S_L is known. First, the "sub-adiabatic" burning velocities of $H_2 + O_2 + N_2$ mixture were determined by extrapolation from sub-adiabatic data points. For each point $c_r{}^i$ of the dependence in Fig. 6, the higher values, i.e. $c_r > c_r{}^i$; $V_g > V_g{}^i$, were removed and the corresponding burning velocities were determined by extrapolation. The obtained function, $S_L{}^i(c_r{}^i)$, is shown in Fig. 8. The real burning velocity of the $H_2 + O_2 + N_2$ mixture is plotted with the error bars representing uncertainty of the TC scattering. Then, the c_r value of the last available experimental point from the corresponding H_2 + air flame, $c_r{}^{max}$, is found on the obtained curve by linear interpolation. The $c_r{}^{max}$ is shown in Fig. 8 with a circle, and the error bars of the H_2 + air S_L are also given for comparison. Assuming that the shape of c_r curves in H_2 + air and $H_2 + O_2 + N_2$ mixtures is not significantly different, the extrapolation uncertainty in S_L can be estimated by looking at $S_L{}^i$ values in the domain $c_r{}^{max} < c_r{}^i < 0$. This extrapolation uncertainty, denoted in the figures as $\Delta S_L{}^e$, was estimated as the difference between the maximum and minimum observed $S_L{}^i$. For the higher unburned gas temperatures, $T_g = 338$ K, 358 K, where the real burning velocity in $H_2 + O_2 + N_2$ mixtures itself was in fact "sub-adiabatic" and found by extrapolation, an additional error, $\Delta S_L{}^{add}$, was added to $\Delta S_L{}^e$ (see figures in the Supplemental Material). Based on all available $S_L{}^i$ dependencies, it was estimated that

if the highest available value of $c_r{}^i$ is larger than -0.1 K s/cm^3, then $\Delta S_L{}^{add} \approx 0.5$ cm/s, for $c_r{}^i \approx -0.15$ K s/cm^3, $\Delta S_L{}^{add} \approx 1$ cm/s, for $c_r{}^i \approx -0.2$ K s/cm^3, $\Delta S_L{}^{add} \approx 1.5$ cm/s. In the same way, the extrapolation uncertainty was estimated for the H_2 + air mixtures at 278 K, where no measurements in $H_2 + O_2 + N_2$ mixtures were performed due to short or zero extrapolation interval in H_2 + air mixtures. The procedure of the estimation of the extrapolation uncertainty for all mixtures is illustrated in the Supplemental Material by figures similar to Fig. 8.

The extrapolation underpredicts S_L, therefore, the value of $\Delta S_L{}^e$ was added to the positive side of the combined error bar from TC scattering and MFCs. Since the latter factors are independent and each of them is centered around the mean, they were added together as a square sum, so that the final expressions become:

$$\Delta S_L^+ = \left(\left(\Delta S_L^{TC+}\right)^2 + \left(\Delta S_L^{MFC}\right)^2 \right)^{0.5} + \Delta S_L^e, \tag{10}$$

$$\Delta S_L^- = \left(\left(\Delta S_L^{TC-}\right)^2 + \left(\Delta S_L^{MFC}\right)^2 \right)^{0.5}, \tag{11}$$

where superscripts "+" and "-" denote the positive and the negative sides of the corresponding error bars, respectively, $\Delta S_L{}^{TC}$ and $\Delta S_L{}^{MFC}$ are the contributions from TC scattering and flow rate measurement, respectively.

3.3. Uncertainty of the temperature dependence

The temperature dependence in the form of the power exponent α is extracted, by using Eq. (1), from individual burning velocities at several temperatures, $S_L^{T_i}$, as a linear least-square fit in logarithmic coordinates. Since α is a function of $S_L^{T_i}$, i.e. $\alpha = f(S_L^{T_1}, \ldots, S_L^{T_n})$, its uncertainty can be estimated with the error propagation rule. For a simple linear regression in logarithmic coordinates, the uncertainty in α is derived as:

$$\Delta\alpha = \frac{\left(\sum_i \left[\left(ln\frac{T_i}{T_0} - \overline{ln\frac{T_i}{T_0}} \right) \cdot \frac{\Delta S_L^{T_i}}{S_L^{T_i}} \right]^2 \right)^{0.5}}{\sum_i ln^2\frac{T_i}{T_0} - n \cdot \left(\overline{ln\frac{T_i}{T_0}} \right)^2}, \tag{12}$$

where n is the number of data points, $\Delta S_L^{T_i}$ is the uncertainty of the burning velocity at temperature T_i and $\overline{ln\frac{T_i}{T_0}}$ is mean logarithmic normalized temperature:

$$\overline{ln\frac{T_i}{T_0}} = \frac{\sum_i ln\frac{T_i}{T_0}}{n}. \tag{13}$$

The error bars for the power exponent α were obtained using Eq. (12) both for the values measured in the current study and for those based on S_L data from the literature as described in [25]. For the present experimental data, $\Delta S_L^{T_i}$ are asymmetric and consist of the positive and negative components, $\Delta S_L^{T_i+}$ and $\Delta S_L^{T_i-}$. The positive and negative error bars of α were determined by the following method. First, the values of $\Delta S_L^{T_i-}$ and the random components of $\Delta S_L^{T_i+}$, i.e. without extrapolation error $\Delta S_L{}^e$ (see Eq. (10)), were regrouped based on whether they increase or decrease α, which is determined by the sign of the difference $T_i - \overline{ln\frac{T_i}{T_0}}$. Then, Eq. (12) was applied to determine the positive and negative side of the error bar of α. Finally, a quantity $\Delta\alpha^e = \alpha(S_L^{T_i} + (\Delta S_L^e)_i) - \alpha(S_L^{T_i})$, which represents the systematic term in α uncertainty due to S_L extrapolation, was added to the positive side of the error bar, since $(\Delta S_L^e)_i$ are bigger at larger T_i, and therefore, $\Delta\alpha^e$ acts to increase α.

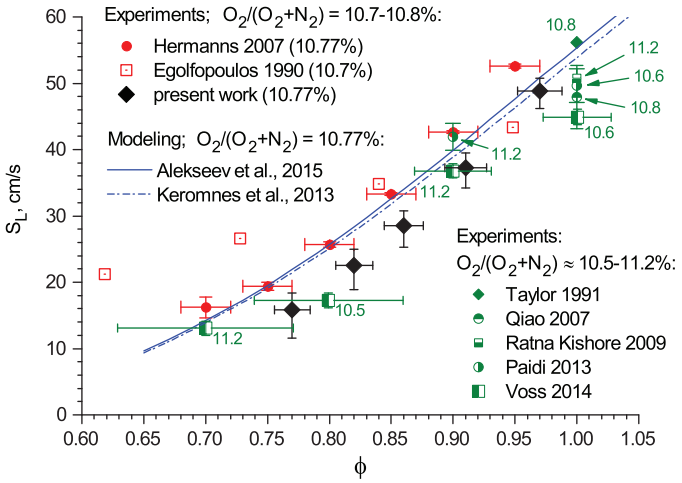

Fig. 9. S_L of $H_2 + O_2 + N_2$ flames at $T_g = 298$ K measured in the present study (black diamonds), taken from the literature: Egolfopoulos and Law [19], Hermanns et al. [37], Taylor [5], Qiao et al. [55], Paidi et al. [56], Voss et al. [39], Ratna Kishore et al. [38] and obtained by kinetic modeling (lines) using reaction schemes from [24,25]. The dilution for the current measurements is $O_2/(O_2 + N_2) = 10.77\%$. The symbols in green were obtained at dilution ratios outside 10.7–10.8% range. (For interpretation of the references to color in this figure legend, the reader is referred to the web version of this article.)

4. Results and discussion

4.1. Reference case: S_L of $H_2 + O_2 + N_2$ flames

Since the diluted mixtures were used in the data processing for H_2 + air flames, as explained in Section 3.2, thus the laminar burning velocities of $H_2 + O_2 + N_2$ mixtures were also determined. The results at $T_g = 298$ K are presented in Fig. 9 in comparison to the available literature data [5,19,37–39,55,56] and kinetic modeling. The S_L values from the present work were obtained by interpolation of the c_r data. In some of the previous studies presented in Fig. 9, the dilution ratio was slightly different from the one considered in the present work, or was varied with ϕ. These data are shown in green color, and specific dilution ratio is given next to the symbol.

Different dilution ratios at which S_L were obtained for different datasets in Fig. 9, to some extent explain the differences between them and in comparison to the present study. Having in mind the influence of dilution on S_L, it can be seen that the current measurements are in agreement with most of the literature data. However, there is some difference between the four sets of experiments performed on heat flux burners: the present, Hermanns et al. [37], Ratna Kishore et al. [38] and Voss et al. [39]. Hermanns et al. [37] show higher values than the other three, even though the agreement between [37] and [38] was observed for lower dilution ratios ($O_2/(O_2 + N_2) = 7.7\%$). The reason for this disagreement is difficult to assess, even though it can be partly explained by uncertainties in equivalence ratio caused by indirect procedure of the MFC calibration implemented in [37].

4.2. Laminar burning velocity of H_2 + air at standard conditions

Figure 10 presents laminar burning velocities of H_2 + air flames at standard conditions (1 atm, 298 K) determined in the present work together with selected set of literature data. The color code is identical to that in Fig. 1. As was discussed in Section 1, the existing scatter in the S_L data at standard conditions can possibly be explained by the data processing methods. For the measurements performed in spherical flames, the results from [17,18] obtained with non-linear stretch correction, are plotted. For the counterflow measurements, since it was shown that burning velocity also varies non-linearly with stretch

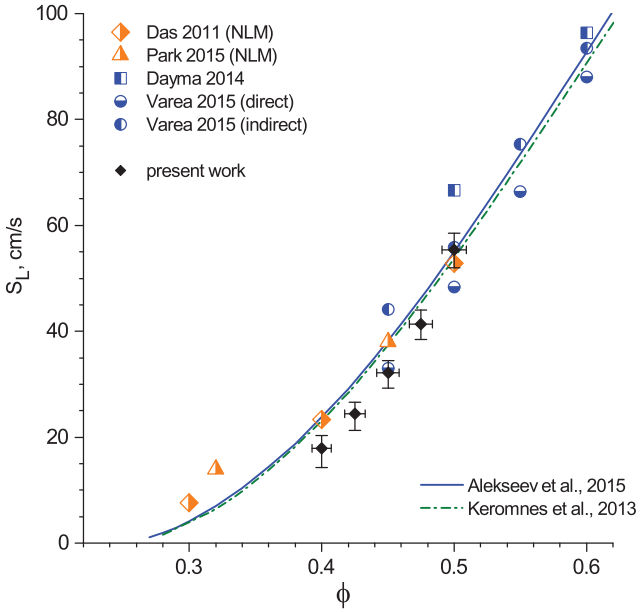

Fig. 10. Laminar burning velocity of lean H_2 + air flames at standard conditions ($T_g = 298$ K, $p = 1$ atm). Symbols: experiments, lines: calculations using models from [24,25]. Experimental: black – current measurements; blue (spherical flame, NLM) – Dayma et al. [17], Varea et al. [18]; orange (counterflow, NLM) – Das et al. [21,22], Park et al. [23]. (For interpretation of the references to color in this figure legend, the reader is referred to the web version of this article.)

[29,30,57], the data from Das et al. [21,22] and Park et al. [23] obtained with the non-linear models of Tien and Matalon [29] and Wang et al. [30], respectively, are shown in the figure. Symbols represent experimental data, while lines show detailed kinetic modeling performed with two contemporary mechanisms for H_2 combustion: the mechanism from our group [25] and the scheme of Keromnes et al. [24].

The S_L values measured in flat flames are generally located below the values obtained in stretched flames for leaner mixtures. This is in agreement with conclusions of Wu et al. [34], who found that for spherical flame configuration, all extrapolation models overpredict S_L, and the effect increases with decreasing ϕ. The present data, however, were found to be in a good agreement with a dataset from the recent experiments in spherical flames by Varea et al. [18]. They presented two sets of data: one was obtained using a technique for direct measurement of the fresh gas velocity before the flame front [58], the second set was obtained by a common method utilizing the density ratio ("indirect" method). The current measurements agree better with the "direct" set at $\phi = 0.45$, and with "indirect" at $\phi = 0.5$. At the higher ϕ one can note that the difference between the two methods of [18] is smaller compared to lower ϕ. For leaner mixtures, $\phi < 0.45$, there are two datasets available, by Das et al. [21,22] and Park et al. [23], performed in the counterflow configuration. The flat flame measurements are found lower than both datasets, and the difference is beyond the evaluated uncertainty for the present results. Moreover, S_L from the present measurements at $\phi = 0.4$ is only slightly above the point of [23] obtained at $\phi = 0.32$. Considering that the stretched flame results processed with the linear model are generally located above non-linear data (See Fig. 1), the flat flames show lower S_L at $\phi < 0.45$ than any of the available literature data. Concerning the comparison with the modeling, experimental results from flat flames disagree with predictions of both mechanisms, which are found to be close to the measurements of Das et al. [21,22].

The results presented above contradict with previous measurements, therefore, in the interpretation of the results it is important to exclude the possibilities of any systematic biases introduced to the data by specific features of the heat flux method. Egolfopoulos et al. [33] in a recent review attributed the effects of radiation, flame-burner interactions, catalytic effects and flame instabilities to such features, apart from those already discussed in Section 3. For the case of hydrogen flames considered in the present study, the effect of H atoms loss on the burner surface and the influence of local flame corrugation come to the fore. The radicals' loss would lower the laminar burning velocity. Hermanns et al. [37] performed kinetic analysis demonstrating that the possible radical sink has very small effect on the value of S_L, by introducing an artificial scavenger of H atoms, which consumed them at the level of the burner plate. Kinetic modeling in the present study shows that the amount of H atoms in the preheat zone in the studied lean H_2 + air mixtures corresponds to that in the mixtures of Hermanns et al. [37] with $O_2/(O_2 + N_2) = 0.0077$ and $\phi \approx 1$–1.7. The fact that S_L for H_2 + air flames determined with the heat flux method possess lower values than available data from stretched flames can thus not be explained by radicals loss on the surface of the burner. The effects of flame corrugation, apart from the fact that they have received special attention in the present work, act to overestimate S_L, so that they can certainly be excluded from consideration of the source of the difference between the flat and stretched flame data. It can be concluded that the difference in the results at 298 K is of fundamental nature.

4.3. S_L at elevated and lowered temperatures

Table 2 presents the measurements performed in the range of temperatures from 278 to 358 K and the extent of extrapolation expressed as $(S_L\text{-}V_{max})/V_{max}$, where V_{max} is the maximal available experimental gas velocity. Also, contribution from extrapolation, $\Delta S_L{}^e$, to the positive error bar is presented. For the S_L uncertainty interval, the positive error $\Delta S_L{}^+$ is given first, then the negative error $\Delta S_L{}^-$.

With the increasing unburned gas temperature, the temperature difference between the gas and the burner plate decreases and consequently, the flame front moves further away from the burner plate. The flames then become less stable, resulting in a decrease of the maximum parabolic coefficient, $c_r{}^{max}$. The extent of extrapolation therefore becomes higher, as evident from Table 2. Concerning the extrapolation uncertainty, from Table 2 it is evident that up to $T_g = 318$ K, the effect of extrapolation is negligible or constitutes a minor fraction of the total positive error bar.

An additional set of measurements was performed at $\phi = 0.375$ and $T_g = 318$–358 K with the aim to cover a wider range for analysis of the temperature dependence. At this equivalence ratio it was impossible to identify the "flat flame" region from the images due to low OH* signal and the velocities were instead filtered based on the shape of the c_r curves. The same procedure was used for the point $\phi = 0.4$ at 278 K. The effect of the instability, i.e. the change of the c_r slope, occurs at higher values of c_r with decreasing ϕ, therefore it can be concluded that the adiabatic conditions for $\phi = 0.4$ at 278 K are still in the "flat flame region", as they are for $\phi = 0.425$. For the data at $\phi = 0.375$ the extrapolation uncertainty was estimated based on the corresponding values from the neighboring points at $\phi = 0.4$ as well as on available c_r dependences at other equivalence ratios.

In the present study it is observed that flame stability for heat flux experiments in H_2 + air flames depends mostly on the temperature difference between the burner plate and unburned mixture. This temperature difference determines the distance between the flame front and the burner, and the trend is in agreement with the conclusions of the numerical studies of Yu et al. [42,59], who identified "a critical stand-off distance" below which the flame can be stabilized on the burner, and with experimental observations in cellular flames of methane [60] and ethane [61] burning in $O_2 + CO_2$ oxidizer. These previous results together with the experimental results of the present work point to the possibility of having flat adiabatic flames of H_2 + air at standard conditions for $\phi = 0.4$–0.5. In the present work this was demonstrated by stabilizing adiabatic flames at lower temperature

Table 2
Laminar burning velocity (S_L) of H_2 + air flames at different unburned gas temperatures, the corresponding extent of extrapolation $(S_L\text{-}V_{max})/V_{max}$ and the extrapolation uncertainty $\Delta S_L{}^e$.

	$S_L \pm \Delta S_L{}^+/\Delta S_L{}^-$, cm/s					$(S_L\text{-}V_{max})/V_{max}$, %					$\Delta S_L{}^e$, cm/s				
ϕ	278 K	298 K	318 K	338 K	358 K	278 K	298 K	318 K	338 K	358 K	278 K	298 K	318 K	338 K	358 K
0.375	–	–	17.2 ± 3.0/3.4	22.1 ± 3.7/1.2	25.8 ± 3.9/0.5	–	–	36	62	89	–	–	1.0	3.0	3.5
0.4	11.7 ± 2.8/4.7	17.9 ± 2.4/3.6	23.0 ± 2.2/2.4	27.4 ± 3.7/1.1	32.0 ± 3.8/0.5	0	7	22	45	52	0	0.2	0.5	2.9	3.3
0.425	18.3 ± 2.4/4.3	24.4 ± 2.2/3.2	29.8 ± 2.0/2.0	35.3 ± 2.2/1.2	41.5 ± 2.5/0.8	0	6	18	29	41	0	0.1	0.5	1.2	1.8
0.45	25.5 ± 2.4/3.8	32.1 ± 2.3/2.9	39.0 ± 2.3/2.1	45.3 ± 3.1/1.5	51.9 ± 3.8/1.0	2	9	20	31	37	0	0.2	0.7	1.9	2.9
0.475	34.0 ± 3.0/3.7	41.3 ± 2.7/2.9	48.9 ± 2.5/2.2	56.7 ± 3.3/1.8	64.5 ± 4.3/1.5	8	12	22	32	40	0.5	0.6	0.8	1.8	3.0
0.5	44.4 ± 3.2/3.6	55.4 ± 3.1/3.4	64.8 ± 2.8/2.6	75.7 ± 3.2/2.0	–	12	17	26	39	–	0.5	0.5	0.8	1.5	–

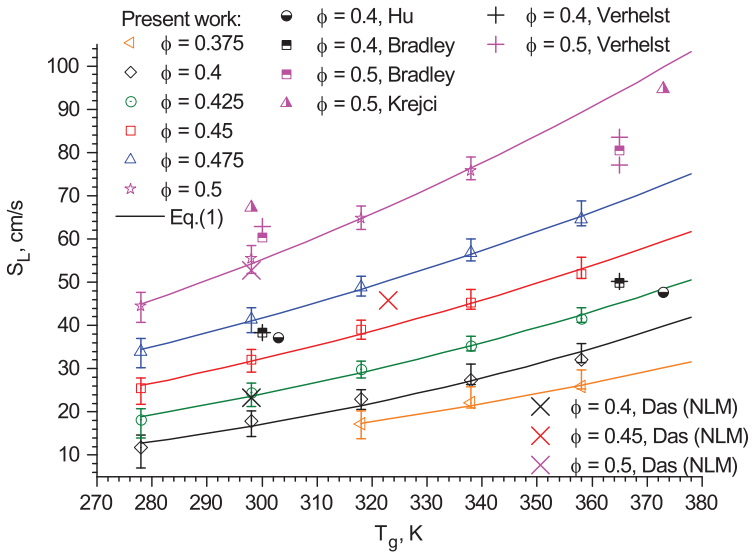

Fig. 11. S_L as a function of unburned gas temperature T_g for different H_2 + air mixtures from the measurements (symbols) and fit with Eq. (1) (lines). Color code: orange – $\phi = 0.375$; black – $\phi = 0.4$; green – $\phi = 0.425$; red – $\phi = 0.45$; blue – $\phi = 0.475$; magenta – $\phi = 0.5$. The data are compared to Hu et al. [13], Bradley et al. [11], Krejci et al. [15], Verhelst et al. [10], Das et al. [21,22]. (For interpretation of the references to color in this figure legend, the reader is referred to the web version of this article.)

of 278 K (see Table 2), i.e., with a larger temperature difference between the gas mixture and the burner plate. For higher T_g, burner plate temperature had to be increased in order to obtain flat adiabatic flames. The temperature range of the current experimental apparatus is limited due to thermal control by water, which can be overcome by changing the working agent to oil.

4.4. Temperature dependence of S_L

Figure 11 presents the laminar burning velocities from Table 2 as a function of the unburned gas temperature for different equivalence ratios (symbols) and fits of the S_L values using Eq. (1) (lines). Figure 11 indicates that the data does not deviate from Eq. (1), i.e. each fit is located within the error bars. Also given in Fig. 11 are the S_L values from the literature obtained in spherical flames [10,11,13,15] with linear extrapolation or in the counterflow burner [21,22] with non-linear model. The colors correspond to a specific equivalence ratio and allow to compare the results from the present work to the literature values.

The power exponent α was determined using the experimental results from the present work, as explained in Section 3.3. The experimentally derived power exponents are presented in Fig. 12 together with the available literature data and kinetic modeling. The experimental and modeled temperature intervals are given in the legend of the Figure or specified explicitly for experimental points at $\phi = 0.375$, 0.5, where they were different. It has to be noted that the presented power exponents are valid within these intervals, since for lean H_2 + air flames α is temperature dependent itself, as discussed in our previous work [25].

The vertical error bars on α from the present study are strongly asymmetrical, higher at the positive side, as a result of larger negative S_L error bars at lower temperatures, and positive error bars at higher temperatures, the latter due to the increased extrapolation uncertainty (See also Fig. 11). Both factors tend to increase α. The largest error bars are at $\phi = 0.375$, this is due to a relatively narrow temperature interval of just 40 K visited at this equivalence ratio: the flames were accessible from 318 to 358 K only. The horizontal error bars in ϕ were adopted from the S_L data, since they solely depend on the flow rates. The difference in S_L itself is large, but due to decreasing gas density and increasing range of extrapolation at higher T_g, the flow rates for each mixture changed in a relatively small range compared to the MFCs full scales. Therefore, the uncertainty in ϕ for each mixture at different T_g is non-independent and can be assumed constant.

Fig. 12 also presents power exponents α from the sources where it was derived directly [10,62–65], and from the studies containing only plots of S_L at room and elevated temperatures [11,13,15,16,21,22,66,67]. For these cases, the error bars were determined in the same way by using Eq. (12). More details on the procedure can be found in our kinetic study of the temperature exponent α in $H_2 + O_2 + N_2$ flames [25], where the difference between the available data in other H_2 flames is also discussed.

Table 3 summarizes temperature exponents α for H_2 + air and diluted flames with corresponding uncertainties, and, as in Table 2, the positive error is given first. Comparing the counterpart mixtures, the values were found to be close to each other, which confirms the validity of the error estimation approach presented in Section 3.2.

The experimental results from the flat flames of the present study provide support for the modeling trend, i.e. the rise of α as the

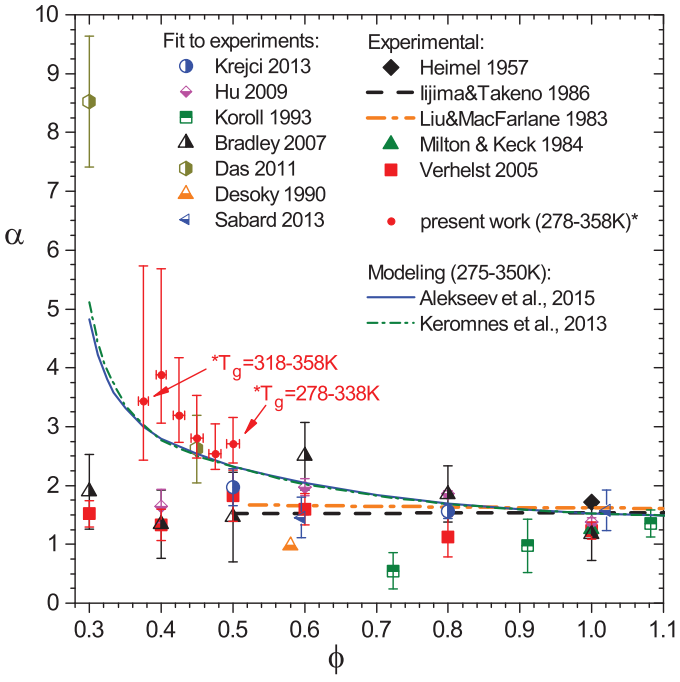

Fig. 12. Temperature exponent α. Red points: present work; solid symbols and thick lines: α taken from the literature: Heimel [62], Iijima and Takeno [63], Liu and MacFarlane [64], Milton and Keck [65], Verhelst et al. [10]; semi-open symbols: α acquired by using S_L data from Krejci et al. [15], Hu et al. [13], Koroll et al. [66], Bradley et al. [11], Das et al. [21, 22], Desoky et al. [67], Sabard et al. [16]; lines: modeling using reaction schemes from [24,25]. (For interpretation of the references to color in this figure legend, the reader is referred to the web version of this article.)

Table 3
Temperature exponent α of H_2 + air and N_2-diluted flames determined in the temperature range T_g.

H_2 + air			$H_2 + O_2 + N_2$		
ϕ	α	T_g, K	ϕ	α	T_g, K
0.375	3.4 ± 2.3/1.0	318–358			
0.4	3.9 ± 1.8/0.8	278–358	0.77	3.7 ± 1.7/0.8	298–358
0.425	3.2 ± 1.0/0.5	278–358	0.82	3.1 ± 1.0/0.6	298–358
0.45	2.8 ± 0.7/0.3	278–358	0.86	2.9 ± 0.7/0.4	298–358
0.475	2.5 ± 0.5/0.3	278–358	0.91	2.6 ± 0.5/0.3	298–358
0.5	2.7 ± 0.5/0.3	278–338	0.97	2.4 ± 0.5/0.4	298–358

mixture gets leaner. Even with comparably large error bars at lower ϕ, as a result of increased relative uncertainty of low S_L, and narrow temperature interval for $\phi = 0.375$, it is evident that α is significantly larger compared to the commonly observed values of $\alpha \approx 1.5$. Most of the available experimental studies indicate α independent on ϕ, except the study of Das et al. [21,22], which is also the only source for α obtained (a) from the measurements using the counterflow burner, and (b) by performing non-linear stretch correction. For the point $\phi = 0.45$, the agreement between the value extracted from the data of [21,22] and the present experimental results is excellent, even though a difference was observed for S_L. The point $\phi = 0.3$ cannot be compared directly, since it was not accessible with our experimental apparatus, i.e. the burning velocities would become too low to achieve a stable flame, $S_L \ll 10$ cm/s (see Fig. 10). In general, α from [21,22] follow the same trend as values from the present study. This is additional evidence of the deviations in spherical flame data obtained with linear extrapolation model, since none of such studies were able to reproduce the modeling trend in α. From Fig. 11 it is seen that S_L is overestimated in the spherical flame studies at room temperature, and at elevated temperatures the results are in a better agreement with the present work. This explains the observed difference in α.

5. Conclusions

Laminar burning velocity of lean H_2 + air flames and its temperature dependence was for the first time measured in flat flames by using the heat flux method. Equivalence ratio was varied in the range $\phi = 0.375$–0.5 and unburned gas temperature was T_g= 278–358 K. With the present experimental apparatus, flat adiabatic flames were stabilized on the burner for $\phi = 0.4$, 0.425 at $T_g = 278$ K, while in other cases flame instabilities became significant before the adiabatic conditions. The transition point where the flames become corrugated was found to be dependent on the temperature difference between the burner plate and the unburned mixture, therefore the possibility of stabilizing flat adiabatic flames at standard conditions in the studied equivalence ratio range is anticipated if burner plate temperature is elevated above 100 °C.

The onset of instabilities was monitored by imaging OH^* emission with a CCD camera, and the recorded dependencies of parabolic coefficient c_r as a function of unburned gas velocity V_g were filtered to include only the values from the stable region, in most cases at sub-adiabatic conditions. The laminar burning velocity was obtained by extrapolation from sub-adiabatic flames with a method similar to the approach of Botha and Spalding [54]. The linearity was validated by application of the same procedure on stable H_2 + air mixtures diluted by N_2 with thermophysical parameters similar to the corresponding H_2 + air mixtures. The extent of extrapolation was analyzed and it was found that for temperatures $T_g \leq 318$ K, its influence on S_L is negligible.

Laminar burning velocity of lean H_2 + air flames at standard conditions was compared to the available literature data and detailed kinetic modeling. The present results are generally located below the values obtained in stretched flames and suggest a different value of the lean flammability limit. This is in agreement with conclusions of Wu et al. [34] who found that for spherical flame configuration, all extrapolation models overpredict S_L. The present data, however, correlates well with most recent experiments in spherical flames of Varea et al. [18] in the overlapping range of equivalence ratios $\phi = 0.45$–0.5. At $\phi < 0.45$ the flat flames show lower S_L than any of the available literature data.

Temperature dependence of the laminar burning velocity was presented for the studied conditions in the form of power exponent α. As opposed to a majority of the previous studies, the data from flat flames supports the trend of increasing α with decreasing ϕ, as predicted by kinetic modeling. It was shown experimentally that α can reach values of about 3–5 at $\phi = 0.4$–0.5. This observation also validates α as an important independent parameter for analysis of reliability and consistency of S_L measurements.

Acknowledgments

The authors would like to acknowledge the financial support from the Centre for Combustion Science and Technology (CECOST). We would also like to thank Professor Chih-Jen Sung and Dr. Apurba Das for providing complementary unpublished results of the H_2 + air burning velocity measurements [22].

Supplementary materials

Supplementary material associated with this article can be found, in the online version, at doi:10.1016/j.combustflame.2015.07.045.

References

[1] J. Warnatz, Combust. Sci. Technol. 26 (1981) 203–213.
[2] G. Dixon-Lewis, Combust. Sci. Technol. 34 (1983) 1–29.
[3] A.L. Sanchez, F.A. Williams, Prog. Energy Combust. Sci. 41 (2014) 1–55.
[4] C.K. Law, F. Wu, F.N. Egolfopoulos, V. Gururajan, H. Wang, Combust. Sci. Technol. 187 (2015) 27–36.

[5] S.C. Taylor, Burning Velocity and the Influence of Flame Stretch, The University of Leeds, 1991 PhD thesis.
[6] V.P. Karpov, A.N. Lipatnikov, P. Wolanski, Combust. Flame 109 (1997) 436–448.
[7] K.T. Aung, M.I. Hassan, G.M. Faeth, Combust. Flame 109 (1997) 1–24.
[8] O.C. Kwon, G.M. Faeth, Combust. Flame 124 (2001) 590–610.
[9] N. Lamoureux, N. Djebaili-Chaumeix, C.-E. Paillard, Exp. Therm. Fluid Sci. 27 (2003) 385–393.
[10] S. Verhelst, R. Woolley, M. Lawes, R. Sierens, Proc. Combust. Inst. 30 (2005) 209–216.
[11] D. Bradley, M. Lawes, K. Liu, S. Verhelst, R. Woolley, Combust. Flame 149 (2007) 162–172.
[12] M.P. Burke, Z. Chen, Y. Ju, F.L. Dryer, Combust. Flame 156 (2009) 771–779.
[13] E. Hu, Z. Huang, J. He, H. Miao, Int. J. Hydrogen Energy 34 (2009) 8741–8755.
[14] M. Kuznetsov, S. Kobelt, J. Grune, T. Jordan, Int. J. Hydrogen Energy 37 (2012) 17580–17588.
[15] M.C. Krejci, O. Mathieu, A.J. Vissotski, S. Ravi, T.G. Sikes, E.L. Petersen, A. Keromnes, W. Metcalfe, H.J. Curran, J. Eng. Gas Turbines Power 135 (2013) Paper 021503.
[16] J. Sabard, N. Chaumeix, A. Bentaib, Fusion Eng. Des. 88 (2013) 2669–2673.
[17] G. Dayma, F. Halter, P. Dagaut, Combust. Flame 161 (2014) 2235–2241.
[18] E. Varea, J. Beeckmann, H. Pitsch, Z. Chen, B. Renou, Proc. Combust. Inst. 35 (2015) 711–719.
[19] F.N. Egolfopoulos, C.K. Law, Proc. Combust. Inst. 23 (1990) 333–340.
[20] C.M. Vagelopoulos, F.N. Egolfopoulos, C.K. Law, Proc. Combust. Inst. 25 (1994) 1341–1347.
[21] A.K. Das, K. Kumar, C.J. Sung, Combust. Flame 158 (2011) 345–353.
[22] A.K. Das, C.J. Sung, private communication.
[23] O. Park, P.S. Veloo, H. Burbano, F.N. Egolfopoulos, Combust. Flame 162 (2015) 1078–1094.
[24] A. Keromnes, W.K. Metcalfe, K.A. Heufer, N. Donohoe, A.K. Das, C.J. Sung, J. Herzler, C. Naumann, P. Griebel, O. Mathieu, M.C. Krejci, E.L. Petersen, W.J. Pitz, H.J. Curran, Combust. Flame 160 (2013) 995–1011.
[25] V.A. Alekseev, M. Christensen, A.A. Konnov, Combust. Flame 162 (2015) 1884–1898.
[26] G.H. Markstein, J. Aeronaut. Sci. 18 (1951) 199–209.
[27] A.P. Kelley, C.K. Law, Combust. Flame 156 (2009) 1844–1851.
[28] C.K. Wu, C.K. Law, Proc. Combust. Inst. 20 (1984) 1941–1949.
[29] J.H. Tien, M. Matalon, Combust. Flame 84 (1991) 238–248.
[30] Y.L. Wang, A.T. Holley, C. Ji, F.N. Egolfopoulos, T.T. Tsotsis, H.J. Curran, Proc. Combust. Inst. 32 (2009) 1035–1042.
[31] F.A. Williams, J.F. Grcar, Proc. Combust. Inst. 32 (2009) 1351–1357.
[32] P.D. Ronney, K.N. Whaling, A. Abbud-Madrid, J.L. Gatto, V.L. Pisowicz, AIAA J. 32 (1994) 569–577.
[33] F.N. Egolfopoulos, N. Hansen, Y. Ju, K. Kohse-Höinghaus, C.K. Law, F. Qi, Prog. Energy Combust. Sci. 43 (2014) 36–67.
[34] F. Wu, W. Liang, Z. Chen, Y. Ju, C.K. Law, Proc. Combust. Inst. 35 (2015) 663–670.
[35] M. Zhou, C.P. Garner, Combust. Flame 106 (1996) 363–367.
[36] S. Balusamy, A. Cessou, B. Lecordier, Exp. Fluids 50 (2011) 1109–1121.
[37] R.T.E. Hermanns, A.A. Konnov, R.J.M. Bastiaans, L.P.H. de Goey, Energy Fuels 21 (2007) 1977–1981.
[38] V. Ratna Kishore, R. Muchahary, A. Ray, M.R. Ravi, Int. J. Hydrogen Energy 34 (2009) 8378–8388.
[39] S. Voss, S. Hartl, C. Hasse, Int. J. Hydrogen Energy 39 (2014) 19810–19817.
[40] M. Goswami, J.G.H. van Griensven, R.J.M. Bastiaans, A.A. Konnov, L.P.H. de Goey, Proc. Combust. Inst. 35 (2015) 655–662.
[41] J.F. Yu, Numerical Study of Cellular Instability in Burner Stabilized Adiabatic Laminar Premixed Flames, Lund University, 2013 PhD thesis.
[42] J.F. Yu, R. Yu, X.S. Bai, Int. J. Hydrogen Energy 38 (2013) 14866–14878.
[43] K.J. Bosschaart, L.P.H. de Goey, Combust. Flame 132 (2003) 170–180.
[44] L.P.H. de Goey, L.M.T. Somers, W.M.M.L. Bosch, R.M.M. Mallens, Combust. Sci. Technol. 104 (1995) 387–400.
[45] R.T.E. Hermanns, Laminar Burning Velocities of Methane-Hydrogen-Air Mixtures, Eindhoven University of Technology, Eindhoven, 2007 PhD thesis.
[46] M. Goswami, K. Coumans, R.J.M. Bastiaans, A.A. Konnov, L.P.H. de Goey, Combust. Sci. Technol. 186 (2014) 1447–1459.
[47] A. van Maaren, D.S. Tsung, L.P.H. de Goey, Combust. Sci. Technol. 96 (1994) 327–344.
[48] K.J. Bosschaart, Analysis of the Heat Flux Method for Measuring Burning Velocities, Technische Universiteit Eindhoven, Eindhoven, 2002 PhD thesis.
[49] K.J. Bosschaart, L.P.H. de Goey, Combust. Flame 136 (2004) 261–269.
[50] T. Knorsch, A. Zackel, D. Mamaikin, L. Zigan, M. Wensing, Energy Fuels 28 (2014) 1446–1452.
[51] L. Sileghem, V.A. Alekseev, J. Vancoillie, K.M. Van Geem, E.J.K. Nilsson, S. Verhelst, A.A. Konnov, Fuel 112 (2013) 355–365.
[52] K.J. Bosschaart, L.P.H. de Goey, Combust. Sci. Technol. 176 (2004) 1537–1564.
[53] Ya.B. Zeldovich, D.A. Frank-Kamenetsky, Compt. Rend. Acad. Sci. USSR 19 (1938) 693.
[54] J.P. Botha, D.B. Spalding, Proc. R. Soc. London, Ser. A. 225 (1954) 71–96.
[55] L. Qiao, Y. Gu, W.J.A. Dahm, E.S. Oran, G.M. Faeth, Combust. Flame 151 (2007) 196–208.
[56] S.K. Paidi, A. Bhavaraju, M. Akram, S. Kumar, Int. J. Hydrogen Energy 38 (2013) 13812–13821 (2013).
[57] G. Dixon-Lewis, Proc. Combust. Inst. 23 (1990) 305–324.
[58] E. Varea, V. Modica, A. Vandel, B. Renou, Combust. Flame 159 (2012) 577–590.
[59] J.F. Yu, R. Yu, X.Q. Fan, M. Christensen, A.A. Konnov, X.S. Bai, Combust. Flame 160 (2013) 1276–1286.
[60] A.A. Konnov, I.V. Dyakov, Exp. Therm. Fluid Sci. 29 (2005) 901–907.
[61] A.A. Konnov, I.V. Dyakov, Combust. Flame 136 (2004) 371–376.
[62] S. Heimel, Effect of initial mixture-temperature on burning velocity of hydrogen-air mixtures with preheating and simulated preburning, Lewis Flight Propulsion Laboratory, 1957 NACA Technical Note 4156.
[63] T. Iijima, T. Takeno, Combust. Flame 65 (1986) 35–43.
[64] D.D.S. Liu, R. MacFarlane, Combust. Flame 49 (1983) 59–71.
[65] B.E. Milton, J.C. Keck, Combust. Flame 58 (1984) 13–22.
[66] G.W. Koroll, R.K. Kumar, E.M. Bowles, Combust. Flame 94 (1993) 330–340.
[67] A.A. Desoky, Y.A. Abdel-Ghafar, R.M. El-Badrawy, Int. J. Hydrogen Energy 15 (1990) 895–905.